

STRUCTURE, MICROSTRUCTURE AND MAGNETO-TRANSPORT PROPERTIES OF $\text{Pr}_{1-x}\text{B}_x\text{CoO}_{3-\delta}$ ($\text{B}^{2+} = \text{Ba}^{2+}, \text{Ca}^{2+}$) PEROVSKITE MATERIALS

B. RIVAS-MURIAS¹, M. SÁNCHEZ-ANDÚJAR¹, J. RIVAS²,
A. FONDADO², J. MIRA² and M.A. SEÑARÍS-RODRÍGUEZ¹

¹*Dpto. Química Fundamental, Universidad da Coruña, 15071 A Coruña, Spain*

²*Dpto. Física Aplicada, Universidad de Santiago, 15706 Santiago de Compostela, Spain*

We have used the “Pechini” method for the efficient preparation of $\text{Pr}_{1-x}\text{B}_x\text{CoO}_3$ ($\text{B}^{2+} = \text{Ba}^{2+}, \text{Ca}^{2+}$) samples. According to the XRD data, the so-obtained samples present an orthorhombic symmetry ($\approx \sqrt{2} a_c \times \approx 2a_c \times \approx \sqrt{2} a_c$) for $x \leq 0.30$ ($\text{B}^{2+} = \text{Ba}^{2+}, \text{Ca}^{2+}$), while the $\text{Pr}_{0.5}\text{Ba}_{0.5}\text{CoO}_3$ compound has a tetragonal symmetry ($a = b \cong a_c$ and $c \cong 2a_c$) and $\text{Pr}_{0.6}\text{Ba}_{0.4}\text{CoO}_3$ is a mixture of an orthorhombic and a tetragonal phase. Nevertheless, in the case of the $\text{Pr}_{0.5}\text{Ba}_{0.5}\text{CoO}_3$ ED reveals the presence of extra order, probably related to the ordering of oxygen vacancies whose number increases with x and is highest for $x = 0.50$. The magnetic and transport properties of these materials change upon doping: as x increases the samples tend to a ferromagnetic behavior and their resistivity tends to diminish. A peculiar magnetotransport behavior is found in the $\text{Pr}_{0.7}\text{Ba}_{0.3}\text{CoO}_3$ and $\text{Pr}_{0.6}\text{Ba}_{0.4}\text{CoO}_3$ compounds.

1. Introduction

The discovery of “colossal” magnetoresistance (CMR) in manganites with perovskite structure has increased the search for new compounds exhibiting such interesting property. In this context cobalt perovskites $\text{Ln}_{1-x}\text{B}_x\text{CoO}_{3-\delta}$ ($\text{Ln}^{3+} = \text{La}^{3+}$, rare earth; $\text{B}^{2+} =$ divalent cation) are very attractive materials in view of the way their magnetic and electrical properties change with temperature and upon doping [Racah et al., 1967; Señarís-Rodríguez et al., 1995 and references therein]. These materials also attract attention due to their high ionic (O^{2-}) conductivity and possible applications in oxygen permeation membranes, fuel cells, etc [Kaga et al., 1990]. Although the strontium-doped lanthanum compounds have been more thoroughly studied [Señarís-Rodríguez et al., 1995], fewer investigations have been carried out on other rare-earth $\text{Ln}_{1-x}\text{B}_x\text{CoO}_{3-\delta}$ systems ($\text{Ln}^{3+} =$ rare earth; $\text{B}^{2+} = \text{Ba}^{2+}, \text{Ca}^{2+}$).

In this paper we refer to the crystal structure, oxygen non-stoichiometry, microstructure and magneto-transport properties of two of these series: $\text{Pr}_{1-x}\text{Ba}_x\text{CoO}_{3-\delta}$ and $\text{Pr}_{1-x}\text{Ca}_x\text{CoO}_{3-\delta}$.

2. Experimental

For the preparation of $\text{Pr}_{1-x}\text{B}_x\text{CoO}_3$ compounds by the “Pechini” method [Licci et al.], Pr_6O_{11} (99.9%, Aldrich) was first converted into the corresponding nitrate by

dissolution in HNO_3 (30%). This product was then added to a 1M citric acid aqueous solution, in which stoichiometric amounts of BaCoO_3 (99+%, Aldrich) or CaCoO_3 (98+%, Panreac) and $\text{Co}(\text{NO}_3)_2 \cdot 6\text{H}_2\text{O}$ (98+%, Aldrich) were also dissolved. After diluting the so-obtained solution, ethylenglicol was carefully added in a proportion 10% v/v. After heating and evaporating the resulting solution at 110°C , the obtained brown gel was decomposed by heating at $400^\circ\text{C}/1\text{h}$. The obtained powders were pressed into pellets and heated in air at 950°C (Ca-series) and 1100°C (Ba-series) during 48h and finally cooled slowly to room temperature ($0.7^\circ\text{C}/\text{min}$)

The samples were characterized by X-ray powder diffraction using a Siemens D-5000 diffractometer and Cu (K_α) = 1.5418 Å radiation. Rietveld analysis of the powder X-ray diffraction data was carried out using the Rietica software suite [Howard et al., 1997]. The morphology and particle size of the polycrystalline samples were studied in a scanning electron microscopy (SEM) using a Jeol 6400 microscope. Electron diffraction studies were carried out on the samples $\text{Pr}_{0.7}\text{Ba}_{0.3}\text{CoO}_{3-\delta}$ and $\text{Pr}_{0.5}\text{Ba}_{0.5}\text{CoO}_{3-\delta}$ in a JEOL 1010 transmission electron microscope operating at 80 kV.

The thermal stability of the samples was checked by differential thermal analysis (DTA) and thermogravimetric analyses (TGA). Iodometric titrations under an argon atmosphere were carried out to analyze the oxygen content of the samples. Magnetic properties were studied in a Squid Quantum Design magnetometer. Zero-field-cooled (ZFC) and field-cooled (FC) magnetic susceptibility data were obtained with an applied field of 1000 Oe from 5 to 330 K. ZFC magnetization curves M (H) were obtained at 5 K using fields of ± 50 kOe. The electrical resistivity, ρ , was measured as a function of temperature in the range $78 \leq T \leq 300$ K in a zero magnetic field using a dc four-probe method employing silver paint contacts or gold sputtered. Seebeck coefficients of pressed pellets were measured in the temperature range $85 \leq T \leq 450$ K. The magnetoresistance of the samples was measured at constant temperature between 0 and 7 kOe.

3. Results and discussion

3.1. SAMPLE CHARACTERIZATION

According to the X-ray diffraction results, we have been able to prepare single-phase crystalline $\text{Pr}_{1-x}\text{B}_x\text{CoO}_3$ compounds with $0 \leq x \leq 0.50$ in the case of $\text{B}^{2+} = \text{Ba}^{2+}$ and with $0 \leq x \leq 0.20$ in the case of $\text{B}^{2+} = \text{Ca}^{2+}$. These polycrystalline materials consist of non completely homogeneous particles with averaged diameter 1-2 μm , as shown by SEM micrographs. Comparatively the Ca-doped samples have a slightly smaller particle size than the Ba-doped compounds due to the lower temperatures used in their synthesis. In these latter materials, sintering between particles is already taking place, resulting in larger plates.

According to the thermogravimetric results, the samples lose some oxygen on heating above 600 K and that loss is more pronounced as x increases. In the case of the lower-doped samples the oxygen can be recuperated almost completely on cooling slowly in air. In comparison the Ca-doped compounds lose less oxygen than their corresponding Ba-doped compounds. The iodometric titrations indicate that the doped-samples are non-stoichiometry in oxygen and that the oxygen deficiency increases with the degree of doping (see Fig. 1). In comparison, the Ca-doped compounds show a smaller oxygen non-stoichiometry. The lattice parameters, atomic coordinates, Co-O bond distances and angles were refined by Rietveld analysis of the powder X-ray diffraction data and the obtained results are given in Table I.

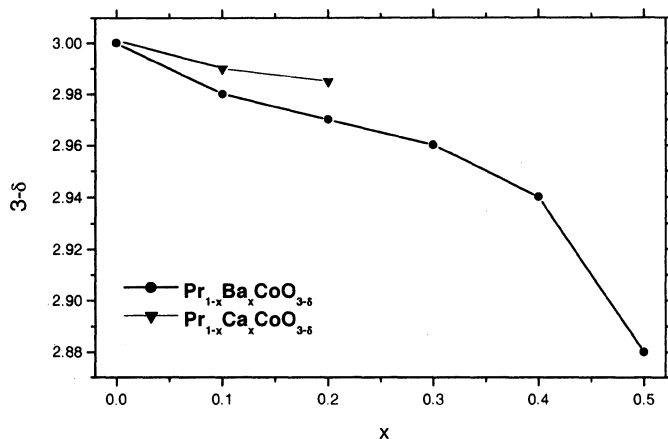


Figure 1. Results of the iodometric titrations under an argon atmosphere.

The X-ray diffraction patterns of the Ba-samples with $x \leq 0.30$ and the Ca-samples with $x \leq 0.20$ can be indexed on the basis of an O-type ($a \leq b/\sqrt{2} \leq c$) orthorhombic GdFeO_3 -like perovskite structure with cell parameters $\approx \sqrt{2} a_c$ ($a_c = 3.8 \text{ \AA}$) $x \approx 2a_c$ $x \approx \sqrt{2} a_c$ (S. G. Pnma) [Radaelli et al., 1997]. Meanwhile, the $\text{Pr}_{0.5}\text{Ba}_{0.5}\text{CoO}_3$ sample presents a tetragonal symmetry with cell parameters $a = b \equiv a_c$ and $c \equiv 2a_c$ (S. G. P4/mmm [Maignan et al., 1999]). Finally, the structure of the $\text{Pr}_{0.6}\text{Ba}_{0.4}\text{CoO}_3$ consist of a mixture of an orthorhombic and a tetragonal phase (Fig. 2).

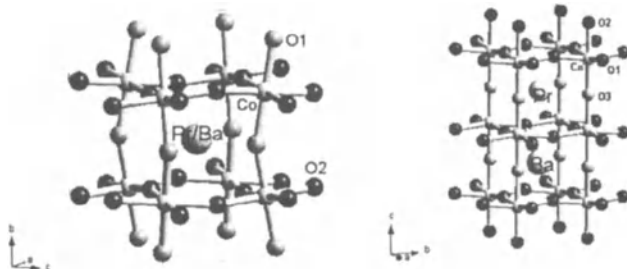


Figure 2. Orthorhombic and tetragonal structures respectively.

To compare the cell parameters of samples with different symmetry we calculate the pseudo-cubic lattice constant (a') that represents the lattice parameter of a cubic unit cell containing one ABO_3 unit and can be defined as $a' = (V/z)^{1/3}$, where V is the volume of the unit cell and z is the number of ABO_3 units in one cell of the crystal ($z=2$ and 4 for a tetragonal and an orthorhombic unit cell, respectively).

It is interesting to note that while this parameter is seeing to increase with x in the Ba-doped samples it almost remain constant in the Ca-series (Fig. 3). This means that in the first case the incorporation of the larger Ba^{2+} cations in place of the smaller Pr^{3+} ions ($r_{\text{Pr}^{3+}}^{\text{XII}} = 1.61 \text{ \AA}$, $r_{\text{Pr}^{3+}}^{\text{XII}} = 1.31 \text{ \AA}$) [Shannon et al., 1969; *ibid*, 1970] predominates

over the fact that upon doping Co^{3+} (${}^{\text{VI}}\text{r}_{(\text{Co})}^{3+} = 0.61 \text{ \AA}$, ${}^{\text{VI}}\text{r}_{(\text{Co})}^{3+} = 0.55 \text{ \AA}$) oxidates to the smaller Co^{4+} ions (${}^{\text{VI}}\text{r}_{(\text{Co})}^{4+} = 0.53 \text{ \AA}$).

TABLE I. Structural parameters obtained from the Rietveld Analysis of the XRD patterns of $\text{Pr}_{1-x}\text{B}_x\text{CoO}_{3-\delta}$ ($\text{B}^{2+} = \text{Ba}^{2+}, \text{Ca}^{2+}$)

ORTHORHOMBIC SYMMETRY: Wyckoff positions Co (0,0,0.5); Pr/B (x,0.25,z); O1 (x,0.25,z); O2 (x,y,z)

Sample		$\text{Pr}_{1-x}\text{Ba}_x\text{CoO}_3$					$\text{Pr}_{1-x}\text{Ca}_x\text{CoO}_3$	
		0.00	0.10	0.20	0.30	0.40	0.10	0.20
Lattice parameter (Å)	a	5.34081	5.37037	5.39635	5.42228	5.42742	5.34812	5.35080
	b	7.57527	7.61239	7.63663	7.66621	7.67144	7.57696	7.57472
	c	5.37628	5.40997	5.44437	5.45998	5.45788	5.37475	5.37202
Atomic coordinates Pr,Ba	x	-0.0290	-0.0218	-0.0094	0.0003	-0.0133	-0.0292	-0.0324
	z	-0.0055	-0.0028	-0.0035	0.0012	-0.0061	-0.0062	-0.0071
Atomic coordinates O1	x	0.5051	0.5059	0.5078	0.4545	0.4413	0.5036	0.5065
	z	0.0667	0.0573	0.0520	-0.0455	-0.0414	0.0615	0.0642
Atomic coordinates O2	x	0.2214	0.2264	0.2289	0.2686	0.2738	0.2199	0.2203
	y	0.0306	0.0331	0.0237	0.0242	0.0242	0.0293	0.0324
	z	-0.2136	-0.2185	-0.2269	0.2700	0.2760	-0.2140	-0.2146
Bond distances (Å)	Co-O1	1.9277	1.9284	1.9305	1.9482	1.9573	1.9230	1.9252
	Co-O2	1.9552	1.9647	1.9419	1.9320	1.9332	1.9482	1.9492
		1.8938	1.9028	1.9229	1.9447	1.9522	1.9016	1.9053
Bond angles (deg)	Co-O1-Co	158.49	161.42	162.92	159.30	156.97	160.16	159.24
	Co-O2-Co	159.75	160.47	165.26	165.93	164.19	159.97	159.19
G. O. F		1.35	1.16	1.24	1.17	1.23	1.31	1.14
R_{Bragg}		1.34	1.86	2.68	2.05	15.30	2.97	1.23
R_p		6.70	9.24	10.84	9.82	10.14	7.58	6.70

TETRAGONAL SYMMETRY: Wyckoff positions Co (0.5,0.5,0.25); Pr (0,0,0.5); B (0,0,0); O1 (0.5,0,z); O2 (0.5,0.5,0); O3

Sample	$\text{Pr}_{1-x}\text{Ba}_x\text{CoO}_3$	
	0.40	0.50
a ≈ b (Å)	3.8939	3.90689
c	7.6378	7.62904
z (O1)	0.2724	0.2217
Co-O1	1.9545	1.9654
Co-O2	1.9094	1.9073
Co-O1-Co	169.94	167.34
Co-O2-Co	179.98	179.98
G. O. F	1.23	1.21
R_{wp}	15.30	16.02
R_p	10.14	10.78

Nevertheless, in the samples doped with the smaller Ca^{2+} ion (${}^{\text{XII}}\text{r}_{(\text{Ca})}^{2+} = 1.34 \text{ \AA}$) the two opposite factors mentioned above just compensate each other and the a' cell parameter changes very little with x. On the other hand, all the ED patterns corresponding to the x=0.30 sample could be indexed on the basis of the orthorhombic cell, as obtained by XRD. Nevertheless the ED patterns of the $\text{Pr}_{0.5}\text{Ba}_{0.5}\text{CoO}_3$ sample reveal that in this case in addition to the average tetragonal structure ($\approx a_c \times \approx a_c \times \approx 2a_c$) different degrees of order are present, as deduced from the presence of extra reflections in the ED patterns, these phenomena give rise to the following news supercells: $\approx a_c \times \approx 2a_c \times \approx 2a_c$ and $\approx 2a_c \times \approx 2a_c \times \approx 2a_c$. The presence of these superstructures is probably

related to an ordering of the oxygen vacancies (that are quite numerous in this compound ($\delta = 0.12$)), as it is commonly observed on other non-stoichiometry oxides [Buseck, 1992] (Fig. 4).

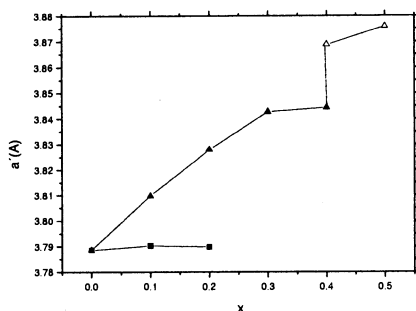


Figure 3. Variation of the pseudo-cubic lattice constant (a') of $\text{Pr}_{1-x}\text{Ba}_x\text{CoO}_3$ (triangles) and $\text{Pr}_{1-x}\text{Ca}_x\text{CoO}_3$ (squares), (filled symbols indicate orthorhombic phase while open symbols indicate tetragonal phase).

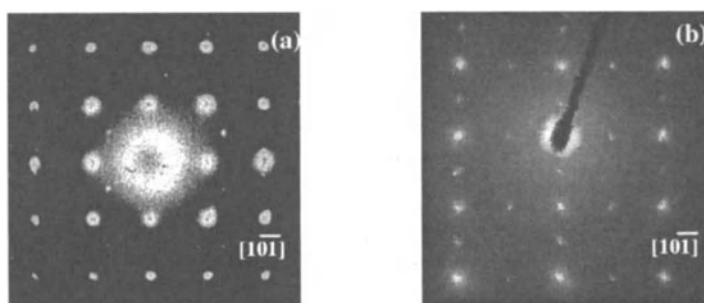


Figure 4. Electron diffraction (ED) patterns of (a) $\text{Pr}_{0.7}\text{Ba}_{0.3}\text{CoO}_3$ and (b) $\text{Pr}_{0.5}\text{Ba}_{0.5}\text{CoO}_3$ samples oriented $[101]$. This pattern is indexed to an unit cell (a) $\approx \sqrt{2} a_c \times 2a_c \times \sqrt{2} a_c$ and (b) $\approx 2a_c \times 2a_c \times 2a_c$.

3.2. MAGNETIC PROPERTIES

While PrCoO_3 is paramagnetic upon substitution of the trivalent Pr^{3+} ions by the divalent $\text{B}^{2+}=\text{Ba}^{2+}, \text{Ca}^{2+}$ ions, the $\text{Pr}_{1-x}\text{B}_x\text{CoO}_3$ materials evolve towards a ferromagnetic behavior (Fig. 5a). It is worth noting that the Curie temperature of the Ba-doped compounds increases slowly with x achieving a maximum value for $x=0.30$ ($T_C=165$ K). This is different from the behavior of $\text{Pr}_{1-x}\text{Sr}_x\text{CoO}_3$ systems where T_C tends to increase upon doping. For $0.30 \leq x \leq 0.50$ the values of T_C in our system are lower than the $\text{Pr}_{1-x}\text{Sr}_x\text{CoO}_3$ samples in the same x region ($T_C > 220$ K) [Yoshii et al., 2000; Brinks et al., 1999].

From the corresponding χ^{-1} (T) fittings we can obtain information about the effective magnetic moment per cobalt ion ($\mu_{\text{eff-Co}}$) and the Weiss constant (θ). The former is calculated from the total $\mu_{\text{eff}} = \sqrt{8C} \mu_B$ after appropriate subtraction of the Pr^{3+} contribution ($\mu_{\text{eff(Pr}^{3+})} = 3.58 \mu_B$) [Morrish, 1965]. In the case of the Ba-samples $\mu_{\text{eff-Co}}$ ranges from 2.7 to 3.4 μ_B . As for their θ , it is seen to increase with x so that the negative values found for lower doping degrees change to positive and higher values with x . In the Ca-doped compounds we observe that the effective magnetic moment per

cobalt ion for $x=0.10$ and 0.20 are slightly higher than in the corresponding Ba-doped compounds and their Weiss constant has negative values. On the other hand, the hysteresis loops (Figure 5b), show that the values of maximum magnetization and remnant magnetization increases with x up to $x=0.30$ and that at 5 K none of them reaches saturation under the field used of $H=50$ kOe.

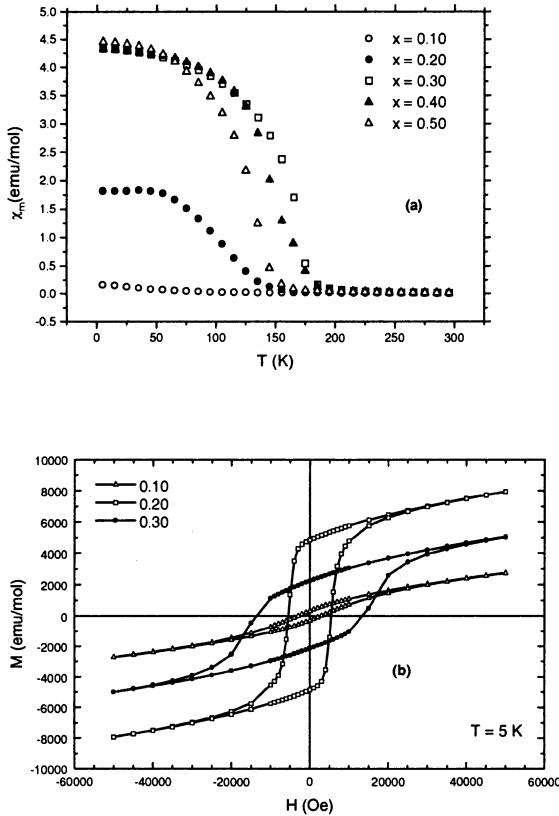


Figure 5. (a) FC molar magnetic susceptibility of $\text{Pr}_{1-x}\text{Ba}_x\text{CoO}_3$ samples ($0 < x \leq 0.50$). and (b) hysteresis loops, measured at 5 K, of $\text{Pr}_{1-x}\text{Ba}_x\text{CoO}_3$ samples ($0 < x \leq 0.30$).

We can also observe that the coercive field achieves a maximum and highest value for $x=0.20$ ($H_c=14100$ Oe) and afterwards it decreases upon further doping. If we now compare the $M(H)$ curves corresponding to the two $\text{Pr}_{1-x}\text{B}_x\text{CoO}_3$ systems ($\text{B}^{2+}=\text{Ba}^{2+}$, Ca^{2+}), we find that for the same degree of doping the values of maximum magnetization, extrapolated magnetization (result of the linear extrapolation of $M(H)$ for higher fields back to $H=0$) and remnant magnetization increase with the size of divalent ion.

3.3. TRANSPORT PROPERTIES

When measuring the resistivity as a function of temperature, $\rho(T)$, the first general observation (that applies to the two series) is that the samples are semiconducting and

their resistivity decreases upon doping. In the case of the Ba-series that decrease occurs progressively up to $x = 0.30$ (see Figure 6), but for further doping resistivity increases again -probably due to the presence of oxygen vacancies- and the metallic regime is never achieved. In both series the electrical conductivity is thermally activated in the temperature range studied. The Seebeck measurements, that indicate again that the electrical conductivity of these samples increases upon doping, also reveal that -except in $\text{Pr}_{0.5}\text{Ba}_{0.5}\text{CoO}_3$ - the charge carriers are holes (the sign of the Seebeck coefficient is positive) and that their number increases with x (Fig. 7).

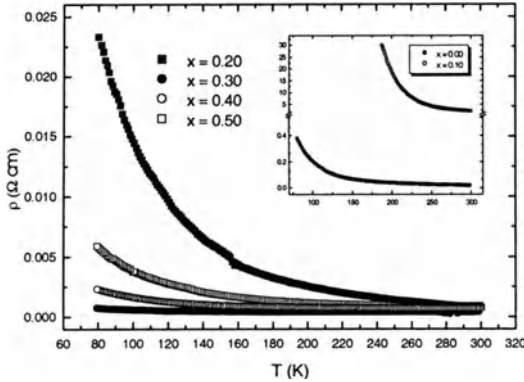


Figure 6. Resistivity versus temperature curves of $\text{Pr}_{1-x}\text{Ba}_x\text{CoO}_3$ samples.

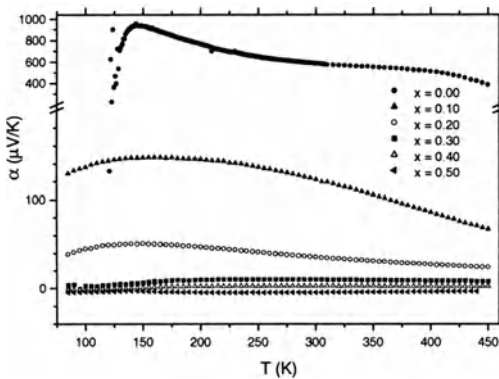


Figure 7. Thermoelectric power, α , of $\text{Pr}_{1-x}\text{Ba}_x\text{CoO}_3$ samples as a function of temperature.

On the other hand, when studying the electrical behavior of these materials under the application of relatively small magnetic fields ($H \leq 8\text{kOe}$) we find peculiar results in the case of the $\text{Pr}_{0.7}\text{Ba}_{0.3}\text{CoO}_3$ and $\text{Pr}_{0.6}\text{Ba}_{0.4}\text{CoO}_3$ compounds: the resistivity of these samples keeps increasing while sweeping the field (Figure 8).

Such a behavior suggest the existence of important relaxation effects in these samples, that seem to be related to the presence of the Pr^{3+} ions. These ions have a big orbital angular momentum ($L=5$) [Morrish, 1965], and give rise to rather high magnetocrystalline anisotropy, and the observed high coercive fields, and could be

involved in a richer dynamic phenomenology under the application of magnetic fields. More work is in progress to completely clarify these surprising and interesting effects.

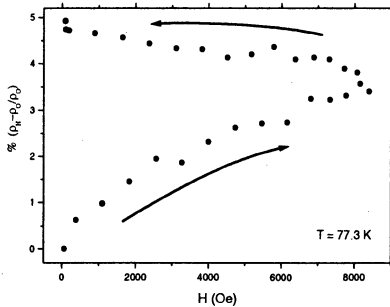


Figure 8. Evolution of the electrical resistivity of the $\text{Pr}_{0.7}\text{Ba}_{0.3}\text{CoO}_3$ sample under the influence of the magnetic field.

Acknowledgements

We thank Spanish DGICYT for financial support under project MAT98-0416-C03-02

References

- Brinks, H.W., Fjellvåg, H., Kjekshus, A. and Hauback, B.C. (1999) *J. Solid State Chem.* **147**, 464.
- Buseck, P., Lowley, J., and Eyring, L. (1992) *High resolution transmission electron microscopy and associated techniques*, Oxford Science Publications, New York.
- Howard, C.J., Hunter, H. and Rietica, B.A. (1997) A Computer Program for Rietveld Analysis of X-ray and Neutron Powder Diffraction Patterns. Australian Nuclear Science and Technology Organization Lucas Heights Research Laboratories.
- Kaga, Y., Ohno, Y., Tsukamoto, K., Uchiyama, F., Lian, M.Y., and Nakajima, T. (1990) *J. Solid State Chem.* **40-41**, 1000 and references therein.
- Licci, F., Besagni, T., and Rinaldi, L. (1985) European Patent, Appl. No. 85860253-2.
- Maignan, A., Martin, C., Pelloquin, D., Nguyen, N., and Raveau, B. (1999) *J. Solid State Chem.* **142**, 247.
- Morrish, A.H. (1965) *The Physical Principles of Magnetism*, Ed. John Wiley & Sons, Inc., New York.
- Raccah, P.M. and Goodenough, J.B. (1967) *Phys. Rev.* **155**, 932.
- Radaelli, P.G., Iannone, G., Marezio, M., Hwang, H.Y., Cheong, S-W., Jorgensen, J.D. and Argyriou, D.N. (1997) *Phys. Rev. B* **56**, 8265.
- Señaris-Rodríguez, M.A. and Goodenough, J.B. (1995) *J. Solid State Chem.* **118**, 323.
- Shannon, R.D. and Prewitt, C.T. (1969), *Acta Crystallogr. B* **25**; *ibid* (1970) **26**, 1046.
- Yoshii, K. and Nakamura, A. (2000) *Physica B* **281&282**, 514.